

**ELECTROWEAK PHYSICS AT CURRENT ACCELERATORS AND
THE SUPERCOLLIDER ***

presented by

U. BAUR [†]*Physics Department**Florida State University, Tallahassee, FL 32306***Working Group Members**U. BAUR^{1‡}, S. ERREDE^{2‡}, F. HALZEN³, S. KELLER¹, G. LANDSBERG⁴, M. L. MANGANO⁵,
A. PERYSHKIN⁶, K. RIESELMANN³, A. STANGE⁷, and D. ZEPPENFELD³¹*Florida State University*, ²*University of Illinois, Urbana – Champaign*, ³*University of Wisconsin, Madison*, ⁴*SUNY at Stony Brook*, ⁵*INFN, Pisa, Italy*, ⁶*Fermilab*, ⁷*Brookhaven National Laboratory***ABSTRACT**

The activities of the Electroweak Physics Working Group are summarized. Three main issues are addressed: 1) prospects for measuring the W mass at the Tevatron using the inclusive electron energy spectrum, 2) constraining the strange quark distribution function in W + charm production, and 3) possibilities to determine the three vector boson couplings at the Tevatron and SSC.

1. Introduction

The study of electroweak processes is one of the main tasks of experiments at current and future accelerators. In order to test the Standard Model (SM) of electroweak interactions its parameters have to be measured as precisely as possible and compared to the SM prediction. Instead of attempting a global analysis of the capabilities of present and future collider experiments, the electroweak working group has focused on the W boson mass and the three vector boson couplings as important parameters to be measured. In addition, the working group has also investigated the prospects of constraining the strange quark distribution function in W plus charm quark production at the Tevatron. The studies reported here are

*To appear in the Proceedings of the Workshop “*Physics at Current Accelerators and the Supercollider*”, Argonne National Laboratory, June 2 – 5, 1993.

[†]Research supported by the U. S. Department of Energy under Contract No. DE-FG05-87ER40319.

[‡]Co-convener

by no means complete. In most cases there is substantial room for improvement left.

The mass of the Z boson is presently known with a precision of about 7 MeV from experiments at LEP [1]. On the other hand, the uncertainty on the W mass from the combined UA2 and CDF data [2] is approximately 270 MeV. Both, UA2 and CDF, used the transverse mass $m_T(\ell, \nu)$, $\ell = e, \mu$ of the charged lepton neutrino system in $W \rightarrow \ell \nu$ decays in the past to determine m_W , a procedure which explicitly depends on measuring the missing transverse momentum, \not{p}_T , in the event. A significant fraction of the overall uncertainty in the W mass, m_W , originates from systematic uncertainties associated with the \not{p}_T measurement. A quantity which is sensitive to m_W but avoids the experimental complications of the \not{p}_T measurement is the lepton energy spectrum. The prospects of using the electron energy distribution as an alternative to the transverse mass for a high precision measurement of m_W were thoroughly investigated [3]. The results of this analysis are described in Section 2.

With the integrated luminosity accumulated during the 1992 – 94 Tevatron collider runs, CDF and DØ expect several thousand $W + 1$ jet events each. For such a large $W + 1$ jet sample it may become possible to search for associated W plus charm quark production. To lowest order Wc production proceeds via the fusion of a gluon and a s or \bar{s} -quark. A measurement of the W plus charm production cross section may thus help in resolving the controversy [4] between the MRS [5] and CTEQ [6] parametrization of the strange quark distribution function. The results of the $W +$ charm analysis are reported in Section 3 [7].

Within the SM, at tree level, the vector boson self-interactions are completely fixed by the $SU(2) \times U(1)$ gauge theory structure of the model. Measuring the $WW\gamma$, $ZZ\gamma$, $Z\gamma\gamma$ and WWZ couplings therefore is a crucial test of the SM. At the Tevatron, this can be accomplished studying $W^\pm\gamma$ and $Z\gamma$ production. Since the number of events expected in run 1a+1b is quite limited, it is important to optimize the statistical procedure used to extract information on the three vector boson vertices. Based on the maximum likelihood technique, a new fitting procedure has been developed [8], which considerably improves upon the simple χ^2 test used in most theoretical simulations [9, 10]. The new technique is summarized in Section 4.1.

A pronounced feature of $W\gamma$ production in hadronic collisions is the so-called radiation zero which appears in the parton level subprocesses which contribute to lowest order in the SM of electroweak interactions [11]. In practice, however, this zero is difficult to observe. The quantity which represents the radiation zero best and, at the same time, is easily measured experimentally is the distribution of the photon – lepton rapidity difference. This quantity was studied extensively in the context of the Workshop [12] (see Section 4.2).

At the Tevatron, the WWV , $V = \gamma, Z$ and $ZZ\gamma$ ($Z\gamma\gamma$) couplings cannot be measured very precisely, due to the limited statistics of di-boson events. High precision tests have to await the SSC or LHC [9, 10]. In order to probe the interactions in the bosonic sector of the SM as accurately as possible, all the important background processes need to be controlled. Furthermore, one would like to have available a large number of basic processes and correspondingly a large number of observables.

A potentially dangerous background to $W^\pm\gamma$ production at hadron supercolliders is $t\bar{t}\gamma$ production. The working group found that the $pp \rightarrow t\bar{t}\gamma + X$ cross section is much larger than the lowest order $W\gamma$ rate; however, imposing a jet veto requirement this background can be eliminated rather easily [13] (see Section 4.3). Besides the classic di-boson production processes $q\bar{q}' \rightarrow W\gamma, WZ$, single W production via the electroweak process $qq \rightarrow qqW$ was studied as a complementary source of information on the three vector boson couplings [14]. A description of the results obtained for the $qq \rightarrow qqW$ signal and the most important background processes can be found in Section 4.4.

2. Measuring the W Boson Mass using the Inclusive Electron Energy Spectrum

The SM has been extraordinarily successful in describing weak and electromagnetic phenomena over the full reach of experimental observation. The model is completely determined by three parameters: the fine structure constant, α , the Fermi constant, G_F , and the Z boson mass, m_Z . All three are known with high precision. With the model so fixed, all other parameters, in particular the W boson mass, m_W , are determined. It is now the task of experiment to carry out precision measurements of m_W to confront the SM prediction.

At hadron colliders, the major problem of the W mass measurement is the neutrino originating from the $W \rightarrow \ell\nu$ decay which escapes undetected. Thus there is no direct way to reconstruct m_W . A standard way to overcome this problem is to use the transverse mass distribution which sharply peaks at m_W . A limiting factor in the determination of m_W from the transverse mass distribution is the systematic uncertainty associated with the determination of the missing transverse momentum, \not{p}_T . Uncertainties originating from the \not{p}_T measurement typically are at least twice as large those from the measurement of the electromagnetic energy.

As an alternative to the transverse mass spectrum, one can try to utilize the lepton energy distribution, which sharply peaks at $m_W/2$ (see Fig. 1 of Ref. 3), and which requires information on the lepton four-momentum only. Two different strategies of extracting m_W from the lepton energy distribution were studied. For definiteness, only the decay $W \rightarrow e\nu$ was considered. In the first approach the energy spectrum is fitted to an analytical function of the form

$$N_e(E) = \frac{N_0}{\Gamma + (E - m_W/2)^2} \quad (1)$$

where N_0 , Γ and m_W are free parameters of the fit which correspond to the number of events, the width and the position of the peak.

In the second approach, a direct comparison of the Monte Carlo electron energy spectrum with the data is carried out, using a Kolmogorov test to compare the two distributions. To estimate the statistical and systematic uncertainties of this method, 10^5 ISAJET $p\bar{p} \rightarrow W \rightarrow e\nu$ events were generated, imposing a $E_t^e > 25$ GeV, a $\not{E}_t > 25$ GeV, and a $|\eta_e| < 1.1$ cut. To simulate detector response the electron momentum four vector was smeared with a Gaussian distribution with standard

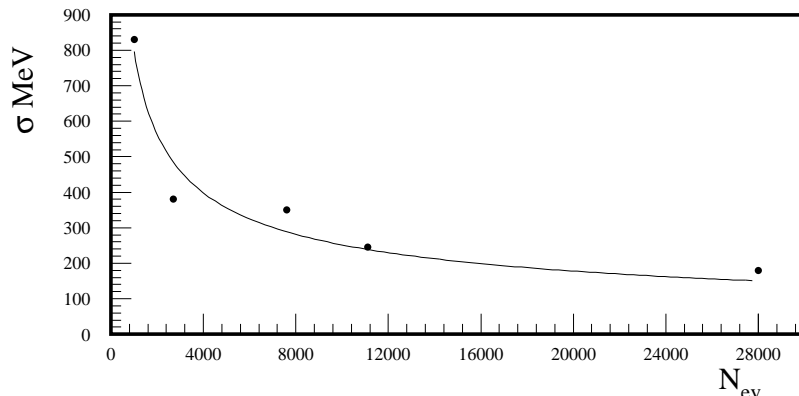


Figure 1: The statistical uncertainty versus number of events, N_{ev} , in the test sample. The solid line shows the result of fitting the uncertainty with the function $P/\sqrt{N_{ev}}$.

deviation $\sigma = 0.15 \text{ GeV}^{1/2} \sqrt{E}$. The MC event sample was split into a “basic” sample of 70,000 events, and a “test” sample which varied from 1,000 to 30,000 events. The statistical uncertainty as a function of the number of events in the test sample is shown in Fig. 1. The solid line corresponds to a fit of the uncertainty of the form $P/\sqrt{N_{ev}}$ where P is a free fit parameter. For 40,000 W events, which roughly corresponds to the number of $W \rightarrow e\nu$ events anticipated at the Tevatron for an integrated luminosity of 100 pb^{-1} , the expected statistical uncertainty is about 125 MeV, and thus about twice as large as the uncertainty from the conventional method employing the transverse mass distribution.

The systematic uncertainties originating from the transverse motion of the W , and from varying the cuts imposed on \cancel{E}_t , E_t^e , and η_e were found to be in the 50 – 100 MeV range each. The expected combined systematic uncertainty is approximately 150 MeV, and thus significantly smaller than that of the conventional method utilizing the transverse mass distribution.

3. The Charm Content of $W + 1$ Jet Events and the Strange Quark Distribution Function

Approximately 15% of the inclusive number of W bosons produced at the Tevatron are accompanied by a hadronic jet with a transverse energy $E_t^{jet} > 15 \text{ GeV}$ [15]. From run 1a and 1b combined one therefore expects more than 6,000 $W + 1$ jet events with $W \rightarrow e\nu$. The large number of W events accompanied by a high p_T jet will make it possible to specifically search for heavy quarks in such events. In particular events for which the jet contains a charm quark could be useful, as they may allow to constrain the strange quark distribution function.

Recent fits of parton distribution functions by the MRS [5] and CTEQ collaborations [6] have resulted in rather different s -quark distribution functions. The ratio of the strange quark distribution functions of the CTEQ1M and the MRSD0 sets versus x_s is shown in Fig. 2a. At small Q^2 and $x_s < 0.1$, the two parametrizations

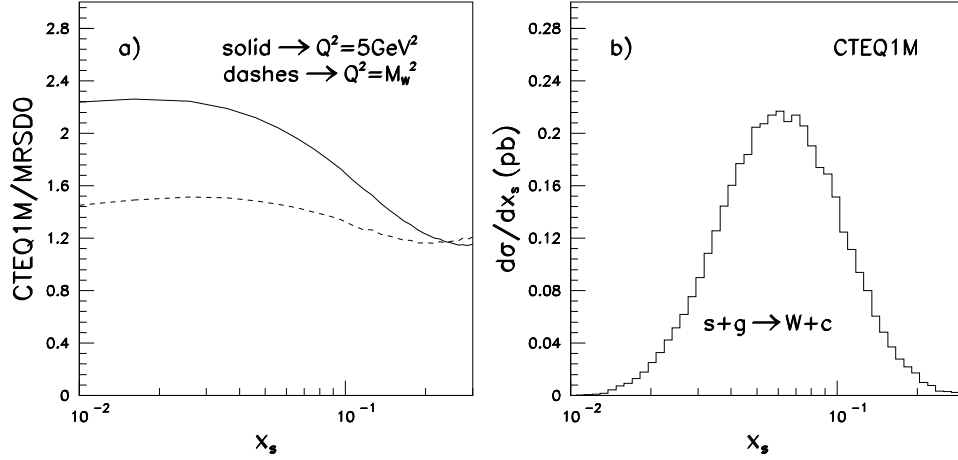


Figure 2: a) Ratio of the strange quark distribution functions as a function of x_s for the CTEQ1M and MRSD0 parton distribution sets and two different values of Q^2 . b) The differential cross section $d\sigma/dx_s$ for the process $sg \rightarrow Wc$ at the Tevatron, using the CTEQ1M set.

differ approximately by a factor of two.

If the charm content of $W + 1$ jet events can be determined, an independent measurement of the strange quark distribution function can be carried out. Associated $W +$ charm production proceeds, at lowest order, through sg and $\bar{s}g$ fusion, $sg \rightarrow W^-c$ and $\bar{s}g \rightarrow W^+\bar{c}$. The alternative process where the s -quark in the reaction is replaced by a d -quark, is suppressed by the quark mixing matrix element V_{cd} . This suppression is somewhat compensated by the larger d quark distribution function, such that the $dg \rightarrow Wc$ cross section is about 10% of the $sg \rightarrow Wc$ rate. The potentially largest background originates from the production of a $c\bar{c}$ pair in the jet recoiling against the W . When only the c or the \bar{c} is identified in the jet, such a $W + c\bar{c}$ event looks like a signal event. Similarly, a $b\bar{b}$ pair can be produced in the jet, and the b or the \bar{b} -quark misidentified as a charm quark.

To numerically simulate the signal and background processes the Monte-Carlo program PYTHIA [16] (version 5.6) was used. All processes were studied at the parton level, *i.e.* final state showers are included but fragmentation is not. In the simulations carried out, a “jet” is defined as follows. The direction of the sum of the momenta of all the partons produced in the shower is taken as the center of a cone of radius $\Delta R_{jet} = \sqrt{\Delta\eta^2 + \Delta\phi^2} = 0.7$, where η is the pseudorapidity and ϕ the azimuthal angle. All the partons inside that cone are considered part of the jet. Only events with a charm quark *inside* the jet cone are counted. Background events with two charm quarks inside the jet cone are counted twice.

The W^\pm is assumed to decay into a $e^\pm\nu$ final state. To simulate the acceptance of a real detector, the following transverse momentum and pseudorapidity

Table 1: Cross sections for associated W plus charm quark production with $W \rightarrow e\nu$ at the Tevatron, using the MRSD0 and CTEQ1M parametrizations of the parton distribution functions. The cuts imposed are summarized in Eq. 2.

	Cross section (pb)				
	Wc	$W + 1$ jet background			Inclusive $W + 1$ jet
	Signal	$g \rightarrow c\bar{c} + X$	$g \rightarrow b\bar{b} + X$	$q \rightarrow qc\bar{c} + X$	
MRSD0	3.68	2.76	0.75	0.15	87.0
CTEQ1M	4.58	2.80	0.77	0.15	85.6

cuts on the final state particles are imposed:

$$\begin{aligned}
p_T(e) &\geq 20 \text{ GeV}, & |\eta(e)| &\leq 1, \\
\not{p}_T &\geq 20 \text{ GeV}, \\
p_T(j) &\geq 10 \text{ GeV}, & |\eta(j)| &\leq 1.
\end{aligned} \tag{2}$$

Figure 2b shows the differential cross section of the process $sg \rightarrow Wc$ for $p\bar{p}$ collisions at $\sqrt{s} = 1.8$ TeV as a function of the momentum fraction of the strange quark, x_s , using the CTEQ1M parametrization. W plus charm quark production at the Tevatron thus is sensitive to the strange quark distribution mostly in the x_s region between 0.04 and 0.1, in which the CTEQ and MRS parametrizations are indeed substantially different (see Fig. 2a).

The cross sections for the signal, the various background processes, and inclusive $W + 1$ jet production at the Tevatron are given in Table 1. Approximately 75% (20%) of the background originates from a $c\bar{c}$ ($b\bar{b}$) pair produced in a jet initiated by a gluon, if all b and \bar{b} -quarks are assumed to be misidentified as charm quarks. The remaining 5% is due to the production of a $c\bar{c}$ pair in a quark-initiated jet. The combined background cross section is about equal to the signal rate. The signal accounts for approximately 4–5% of all $W + 1$ jet events, and the background for about 4%. As can be seen from Table 1, the two sets of parton distribution functions yield the same values for the inclusive $W + 1$ jet cross section and the three background processes to within 2%. The signal rate, on the other hand, is quite sensitive to which set is chosen, as expected.

Assuming both electron and muon decay channel of the W^\pm boson, an integrated luminosity of 10 pb^{-1} yields about 1700 $W + 1$ jet events for the cuts described in Eq. 2. This corresponds to approximately 75 – 90 W plus charm quark signal events, and to about the same number of potential background events. From these numbers it is straightforward to estimate the minimum charm tagging efficiency, ϵ_c^{min} , required to be statistically sensitive to the variation of the Wc production cross section with the strange quark distribution function. Depending on how efficiently the various background processes can be suppressed, an efficiency of $\epsilon_c^{\text{min}} \approx 20 - 30\%$ is needed for an integrated luminosity of 10 pb^{-1} .

The two collider experiments, CDF and DØ, at the Tevatron explore three

different strategies to identify charm quarks:

1. Search for a displaced secondary vertex in the silicon vertex detector (SVX).
2. Reconstruction of exclusive nonleptonic charmed baryon or meson decays.
3. Looking for inclusive semileptonic charm decays.

Combined, the three methods may yield an overall charm detection efficiency of about 10%. Based on this assumption, an integrated luminosity of $\mathcal{O}(30 \text{ pb}^{-1})$ should provide the first statistically significant information on the strange quark distribution of the proton. A more precise estimate of the minimum integrated luminosity required depends on a better understanding of the charm quark detection efficiency, and on more detailed background studies. In principle, the three background processes considered here can be reduced by:

- Charge reconstruction: for the signal, the W and c -quark electric charges are correlated. For the $c\bar{c}$ background, the charm quark has the wrong charge 50% of the time. Therefore, if the charges of the W and of the charm quark can be determined, the $Wc\bar{c}$ background can be reduced by a factor of two. Furthermore, events with the wrong charge correlation provide a measurement of the background, that could subsequently be subtracted.
- Cut on the charm transverse momentum: since more than one charm quark is present in the background processes its average p_T is smaller than in the signal.
- Flavor identification: if the bottom quark is identified, the $b\bar{b}$ background can be subtracted.

Clearly, more experimental and theoretical work is needed to improve the signal to background ratio.

4. Probing the Vector Boson Self-interactions in Hadron Collider Experiments

4.1 Extracting Three Vector Boson Couplings from the Photon Transverse Momentum Distribution

The increased integrated luminosity accumulated in the 1992 – 94 Tevatron collider runs will not only make it possible to improve the precision of existing measurements, but also to probe previously untested sectors of the SM, such as the self-interactions of vector bosons. This is most easily done studying $W\gamma$ and $Z\gamma$ production.

The most general $WW\gamma$ vertex function for $q\bar{q}' \rightarrow W\gamma$ which is compatible with electromagnetic gauge invariance and Lorentz invariance, and which is CP conserving, can be parameterized in terms of two couplings κ^γ and λ^γ [9]. Similarly, under the same conditions, the $ZZ\gamma$ and $Z\gamma\gamma$ vertex can be described by two

couplings, h_3^V and h_4^V , $V = \gamma, Z$. In the SM, at tree level, $\kappa^\gamma = 1$, $\lambda^\gamma = 0$, and $h_3^V = h_4^V = 0$. In order to avoid violations of S -matrix unitarity, the anomalous three vector boson couplings have to be introduced as momentum dependent form factors. Frequently, generalized dipole form factors of the form

$$a(\hat{s}) = \frac{a_0}{(1 + \hat{s}/\Lambda^2)^n} , \quad (3)$$

with $a = \kappa^\gamma - 1, \dots, h_4^V$ are used. Λ in Eq. (3) represents the scale at which new physics becomes important in the weak boson sector, \hat{s} is the energy squared in the parton center of mass frame, and a_0 are the form factors at low energy. In order to guarantee unitarity, n must satisfy $n > 1/2$ for $\Delta\kappa^\gamma = \kappa^\gamma - 1$, $n > 1$ for λ^γ , $n > 3/2$ for h_3^V , and $n > 5/2$ for h_4^V .

Non-standard $WW\gamma$ and $ZZ\gamma$ ($Z\gamma\gamma$) couplings lead to a broad increase in the photon transverse momentum distribution at large values of the photon p_T [9, 10]. Information on the anomalous three vector boson couplings thus can be derived by fitting the observed $p_T(\gamma)$ distribution with general $WW\gamma$ and $ZZ\gamma$ ($Z\gamma\gamma$) couplings.

The main background for $p\bar{p} \rightarrow W\gamma, Z\gamma$ is $W + jets$ and $Z + jets$ production with one of the jets faking a high p_T photon due to fragmentation of the jet into a high energy π^0 or η , which decays into two almost collinear photons which are not resolved in the detector. This background rapidly drops with the γ/jet transverse momentum. The probability $P_{\gamma/j}$ for the jet faking a photon has been measured by CDF and DØ separately. Both collaborations find $P_{\gamma/j} \approx 10^{-3}$ for $p_T(\gamma) > 10$ GeV. Electrons misidentified as photons due to tracking inefficiencies may also constitute a non-negligible background for DØ.

In most theoretical simulations [9, 10], a rather primitive procedure for fitting the photon p_T spectrum was used. In this procedure the distribution is split into a number of bins of equal bin width plus one additional bin which contains all events above a certain p_T threshold. This threshold is chosen such that each bin contains typically more than 5 events. In each bin, the Poisson statistics is then approximated by a Gaussian distribution, and a minimum χ^2 test is performed.

A substantial improvement of this method can be achieved, especially for low statistics, by two simple modifications:

1. Replace the Gaussian distribution and the χ^2 test by Poisson statistics and a maximum likelihood fit. In contrast to the χ^2 method, the maximum likelihood technique yields unbiased estimates of the fitted parameters.
2. An extra bin, in which one would not expect any SM events at the 95% confidence level (CL) is added. This modification fully exploits the enhancement of the differential cross section at large $p_T(\gamma)$ values for anomalous couplings.

The results of applying the improved fitting procedure to the data sets expected for DØ are summarized in Table 2. They are up to a factor 2 better than those derived using the χ^2 test. The limits for $\Delta\kappa_0^\gamma$ (h_3^Z) apply for arbitrary values of λ_0^γ

Table 2: Expected limits from $D\bar{O}$ for the CP conserving $WW\gamma$ and $ZZ\gamma$ couplings. The limits for the $ZZ\gamma$ couplings are derived using $n = 3$ ($n = 4$) for h_3^Z (h_4^Z) and a form factor scale of $\Lambda = 750$ GeV. The bounds on the $WW\gamma$ couplings $\Delta\kappa^\gamma$ and λ^γ are insensitive to the form factor details. Both, the electron and muon decay channels for the W and Z boson are used.

Coupling	run 1a limits		run 1a+1b limits	
	68% CL	95% CL	68% CL	95% CL
$ \Delta\kappa_0^\gamma $	1.10	2.50	0.60	1.15
$ \lambda_0^\gamma $	0.30	0.75	0.15	0.31
$ h_{30}^Z $	0.62	1.27	0.38	0.72
$ h_{40}^Z $	0.10	0.21	0.06	0.11

(h_{40}^Z) and vice versa. Bounds on h_{30}^γ (h_{40}^γ) are approximately 10% weaker than those for h_{30}^Z (h_{40}^Z).

4.2 Rapidity Correlations in $W\gamma$ Production

A pronounced feature of $W\gamma$ production in hadronic collisions is the so-called radiation zero which appears in the parton level subprocesses which contribute to lowest order in the SM of electroweak interactions [11]. For $u\bar{d} \rightarrow W^+\gamma$ ($d\bar{u} \rightarrow W^-\gamma$) all contributing helicity amplitudes vanish for $\cos\Theta^* = -1/3$ ($+1/3$), where Θ^* is the angle between the quark and the photon in the parton center of mass frame. In practice, however, this zero is difficult to observe. Structure function effects transform the zero into a dip. Higher order QCD corrections [10, 17] and finite W width effects, together with photon radiation from the final state lepton line, tend to fill in the dip. Finally, the twofold ambiguity in the reconstructed parton center of mass frame which originates from the two possible solutions for the longitudinal momentum of the neutrino [18], $p_L(\nu)$, represents an additional complication in the extraction of the $\cos\Theta^*$ or the corresponding rapidity distribution, $d\sigma/dy^*(\gamma)$, which further dilutes the effect.

Photon lepton rapidity correlations provide an alternative tool to search for the radiation zero predicted by the SM for $W\gamma$ production in hadronic collisions. For the remainder of this subsection we shall focus entirely on the $W^+\gamma$ channel. Results for $W^-\gamma$ production can be obtained by simply exchanging the sign of the rapidities involved. The SM radiation zero leads to a pronounced dip in the photon rapidity distribution in the center of mass frame, $d\sigma/dy^*(\gamma)$, at

$$y^*(\gamma) = y_0 = -\frac{1}{2} \log 2 \approx -0.35. \quad (4)$$

For $u\bar{d} \rightarrow W^+\gamma$ the photon and the W are back to back in the center of mass frame. The corresponding rapidity distribution of the W in the parton center of mass frame, $d\sigma/dy^*(W)$, thus exhibits a dip at $y^*(W) = -y_0$. In the double differential distribution of the rapidities in the laboratory frame, $d^2\sigma/d\eta(\gamma)dy(W)$, one then

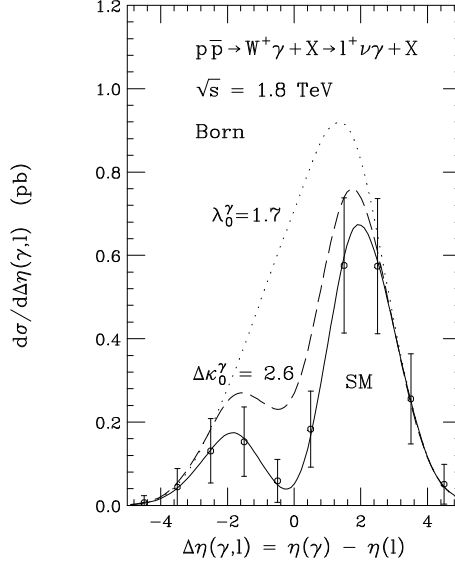


Figure 3: The rapidity difference distribution, $d\sigma/d\Delta\eta(\gamma, \ell)$, for $p\bar{p} \rightarrow W^+\gamma + X \rightarrow \ell^+\not{p}_T\gamma + X$, $\ell = e, \mu$, at the Tevatron in the Born approximation for anomalous $WW\gamma$ couplings. The curves are for the SM (solid), $\Delta\kappa_0^\gamma = 2.6$ (dashed), and $\lambda_0^\gamma = 1.7$ (dotted). Only one coupling is varied at a time. A dipole form factor with scale $\Lambda = 1$ TeV is assumed for non-standard $WW\gamma$ couplings. The cuts imposed are described in the text. The error bars indicate the expected statistical uncertainties for an integrated luminosity of 22 pb^{-1} .

expects a “valley” or “channel” for rapidities satisfying the relation[§] $\eta(\gamma) - y(W) \equiv y^*(\gamma) - y^*(W) = 2y_0$.

In the SM, the dominant W^\pm helicity in $W\gamma$ production is $\lambda_W = \pm 1$ [19], implying that the charged lepton will tend to be emitted in the direction of the parent W , thus reflecting most of its kinematic properties. The difference in rapidity, $\Delta y(W, \ell) = y(W) - \eta(\ell)$, between the W boson and the charged lepton originating from the W decay is rather small with an average $\Delta y(W, \ell)$ of 0.30. The double differential distribution $d^2\sigma/d\eta(\gamma)d\eta(\ell)$ for $p\bar{p} \rightarrow W^+\gamma \rightarrow \ell^+\not{p}_T\gamma$ thus displays a channel for rapidities fulfilling the relation $\Delta\eta(\gamma, \ell) = \eta(\gamma) - \eta(\ell) \approx -0.4$.

The double differential distribution $d^2\sigma/d\eta(\gamma)d\eta(\ell)$ can only be mapped out if a sufficiently large number of events is available. For a relatively small event sample the distribution of the rapidity difference, $d\sigma/d\Delta\eta(\gamma, \ell)$, which is shown in Fig. 3, is more useful. Here a $p_T(\gamma) > 5$ GeV, a $p_T(\ell) > 20$ GeV and a $\not{p}_T > 20$ GeV cut are imposed, together with cuts on the pseudorapidities of the photon and charged lepton of $|\eta(\gamma)| < 3$ and $|\eta(\ell)| < 3.5$. To select a phase space region where radiative W decays are suppressed and $q\bar{q}' \rightarrow W\gamma$ dominates, we have required in addition a large photon lepton separation cut of $\Delta R(\gamma, \ell) > 0.7$, and a cluster transverse mass cut of $m_T(\ell\gamma; \not{p}_T) > 90$ GeV. The solid line shows the SM result, whereas the dashed

[§]Differences of rapidities are invariant under boosts.

and dotted curves give the prediction for the current UA2 68% CL limits [20] of $\Delta\kappa_0^\gamma = 2.6$ and $\lambda_0^\gamma = 1.7$, respectively. In Fig. 3, a dipole form factor ($n = 2$) with a scale $\Lambda = 1$ TeV was used.

As anticipated, the $\Delta\eta(\gamma, \ell)$ distribution exhibits a strong dip at $\Delta\eta(\gamma, \ell) \approx -0.4$ in the SM (solid line). Higher order QCD corrections fill in the dip partially, but do not obscure the radiation zero in a significant way. Compared to $d\sigma/dy^*(\gamma)$, the rapidity difference distribution has the advantage of being independent of the twofold ambiguity in the reconstruction of the parton center of mass frame, which considerably obscures the radiation zero in the $y^*(\gamma)$ distribution. In contrast to the $Z\gamma$ to $W^\pm\gamma$ cross section ratio which also reflects the radiation zero [21], the rapidity difference distribution does not depend on the $Z\gamma$ cross section, and the validity of the SM for $p\bar{p} \rightarrow Z\gamma$.

In presence of any anomalous contribution to the $WW\gamma$ vertex the radiation zero is eliminated and the dip in $d\sigma/d\Delta\eta(\gamma, \ell)$ is filled in at least partially. Most of the excess cross section for non-standard couplings originates in the high $p_T(\gamma)$ region [9], where events tend to be central in rapidity. Deviations from the SM $\Delta\eta(\gamma, \ell)$ distribution, therefore, mostly occur for small rapidity differences. In Fig. 3 we have also included the statistical uncertainties expected in the SM case for an integrated luminosity of $\int \mathcal{L} dt = 22 \text{ pb}^{-1}$. This demonstrates that the rapidity difference distribution is sensitive to anomalous $WW\gamma$ couplings already with the current CDF and DØ data samples, in particular to λ^γ . However, one does not expect $d\sigma/d\Delta\eta(\gamma, \ell)$ to be more sensitive to anomalous couplings than the photon transverse momentum distribution.

4.3 The $t\bar{t}\gamma$ Background in $W\gamma$ Production at the SSC

Whereas the three vector boson couplings can be measured only at the 10 – 60% level at best at the Tevatron (see Section 4.1), the SSC or LHC provide the energy and luminosity necessary for a high precision test of these couplings. However, for $W\gamma$ production the process $pp \rightarrow t\bar{t}\gamma \rightarrow W\gamma + X$ represents a potentially dangerous background, due to the very large top quark production cross section at supercollider energies. In this subsection a calculation of the $t\bar{t}\gamma$ background at the SSC is described. The calculation fully incorporates the subsequent decay of the top quarks into a W boson and a b -quark, and also the W decay into a fermion antifermion pair. Graphs where the photon is radiated from one of the t or \bar{t} decay products are not taken into account. The contribution from these diagrams is strongly suppressed if a photon p_T cut of $p_T(\gamma) > m_t/2$ is imposed. The top quark and W boson decays are treated in the narrow width approximation.

Besides the lowest order contributions to the associated production of a $t\bar{t}$ pair and a photon, the photon bremsstrahlung contribution in $t\bar{t}j$ events is included in our calculation. The bremsstrahlung contribution is calculated using the QCD $q\bar{q} \rightarrow t\bar{t}g$, $qg \rightarrow t\bar{t}q$ and $g\bar{g} \rightarrow t\bar{t}g$ matrix elements together with the leading-logarithm parametrization of Ref. [22] for the photon fragmentation functions. These fragmentation functions are proportional to α/α_s , and the photon bremsstrahlung contribution formally is of the same order in α as the lowest order $t\bar{t}\gamma$ cross section.

In the following only the channel $pp \rightarrow W^+\gamma + X$ is considered. The cross sections of the $t\bar{t}\gamma$ background are equal for the $W^+\gamma + X$ and $W^-\gamma + X$ channel. The $pp \rightarrow W^-\gamma + X$ signal rate is approximately 20% smaller than the $pp \rightarrow W^+\gamma + X$ cross section for the cuts specified below. The conclusions drawn for the $W^+\gamma$ case therefore also apply to the $W^-\gamma$ channel.

The W^+ boson is assumed to decay into a $\ell^+\nu$ final state with $\ell = e, \mu$. In order to simulate the finite acceptance of detectors and to reduce fake backgrounds from jets misidentified as photons and particles lost in the beam pipe [23], the following transverse momentum, pseudorapidity and separation cuts are imposed:

$$p_T(\ell^+) > 25 \text{ GeV}, \quad |\eta(\ell^+)| < 3.0, \quad (5)$$

$$p_T(\gamma) > 100 \text{ GeV}, \quad |\eta(\gamma)| < 2.5, \quad (6)$$

$$\not{p}_T > 50 \text{ GeV}, \quad \Delta R(\ell^+, \gamma) > 0.7. \quad (7)$$

No cuts are imposed on the b -quark jets and the decay products of the second W (*i.e.* the W^-) in $t\bar{t}\gamma$ events. $W^- \rightarrow \tau\nu_\tau$ decays are, for simplicity, treated like $W^- \rightarrow e\nu, \mu\nu$.

Figure 4a shows the $p_T(\gamma)$ distribution for $pp \rightarrow t\bar{t}\gamma + X \rightarrow \ell^+\not{p}_T\gamma + X$ at the SSC for $m_t = 110 \text{ GeV}$ (solid line) and $m_t = 200 \text{ GeV}$ (dashed line). The photon bremsstrahlung cross section is approximately 40 – 65% of the lowest order $pp \rightarrow t\bar{t}\gamma$ rate over the entire $p_T(\gamma)$ range shown in Fig. 4a. The shape of the photon transverse momentum distribution depends on the top quark mass, with the $p_T(\gamma)$ distribution becoming harder for increasing values of m_t . The dotted curve in Fig. 4a shows the lowest order prediction of the photon p_T distribution for the $W^+\gamma$ signal. The $t\bar{t}\gamma$ background is seen to be much larger than the cross section of the signal over the entire top quark mass range studied. It is obvious from Fig. 4a that the $t\bar{t}\gamma$ background will considerably reduce the sensitivity of the reaction $pp \rightarrow W^+\gamma + X$ to non-standard $WW\gamma$ couplings.

Since the top quark decays predominantly into a Wb final state, $t\bar{t}\gamma$ events are characterized by a large hadronic activity which frequently results in one or several high p_T jets. This observation suggests that the $t\bar{t}\gamma$ background may be suppressed by vetoing high p_T jets. Such a “zero jet” requirement has been demonstrated [10] to be very useful in reducing the size of NLO QCD corrections in $pp \rightarrow W\gamma + X$ at SSC energies. Present studies [23] suggest that for $p_T(j) < 35 \text{ GeV}$ SSC detectors face increasing difficulties in reconstructing jets. Requiring that *no* jets with $p_T(j) > 35 \text{ GeV}$ and *no* second charged lepton are observed for $|\eta(j)|, |\eta(\ell)| < 3$, and that the photon is isolated from the hadronic activity, one obtains the results shown in Fig. 4b. The $t\bar{t}\gamma$ background is seen to be about one order of magnitude below the signal (dotted line) for $m_t = 110 \text{ GeV}$ (solid line), and approximately two orders of magnitude for $m_t = 200 \text{ GeV}$ (dashed line).

4.4 Measuring Three Vector Boson Couplings in $qq \rightarrow qqW$ at the SSC.

In order to probe the vector boson self interactions as completely as possible one would like to have available a large number of basic processes and correspondingly a large number of observables. As an example of a new process which is

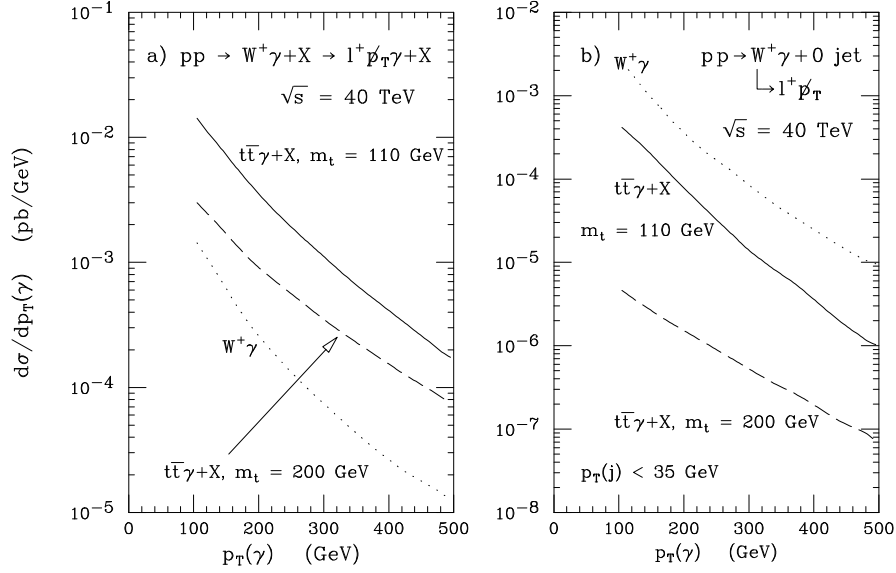


Figure 4: a) The photon transverse momentum distribution for $pp \rightarrow W^+\gamma + X \rightarrow \ell^+ \not{p}_T \gamma + X$ at the SSC. The solid (dashed) line shows the result for $t\bar{t}\gamma + X$ production for $m_t = 110$ GeV (200 GeV). The dotted line gives the tree level SM prediction of the $W^+\gamma$ signal. The cuts imposed are summarized in Eqs. (5) – (7). b) The photon transverse momentum distribution for $pp \rightarrow W^+\gamma + 0 \text{ jet} \rightarrow \ell^+ \not{p}_T \gamma + 0 \text{ jet}$ at the SSC with a jet transverse momentum threshold of 35 GeV. The solid (dashed) line shows the result for the $t\bar{t}\gamma$ background for $m_t = 110$ GeV (200 GeV). The dotted line gives the NLO prediction of the $p_T(\gamma)$ distribution for the $W^+\gamma + 0 \text{ jet}$ signal in the SM.

complementary to weak boson pair production in the measurement of the $WW\gamma$ and WWZ vertices, the working group investigated single W production via the electroweak process $qq \rightarrow qqW$. While $W\gamma$, WZ , or W^+W^- production at hadron or e^+e^- colliders probe the three vector boson couplings for time-like momenta of all interacting electroweak bosons, the signal process measures these couplings for space-like momentum transfer of two of the three gauge bosons.

The signal and all background cross sections were calculated using parton level Monte Carlo programs. For the signal the program evaluates the tree level cross sections for the process $q_1 q_2 \rightarrow q_3 q_4 \ell \nu$, $\ell = e, \mu$ and all relevant crossing related processes. Representative Feynman graphs are shown in Fig. 5. A characteristic feature of the W signal is the presence of two energetic forward jets. However,

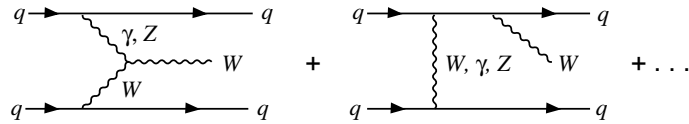


Figure 5: Feynman graphs for the $qq \rightarrow qqW$ signal. It is via the first graph that this process is sensitive to the three vector boson couplings.

anticipating large backgrounds, all the features of the final state Wjj system need to be exploited for background suppression. Therefore, the signal is only considered in the case when both final state (anti)quarks have transverse momenta larger than 40 GeV, allowing their identification as hadronic jets. The potentially most dangerous background processes are QCD Wjj and $t\bar{t}$ production. The dominant source of forward jets in $t\bar{t}$ events arises from QCD radiation, *i.e.* the additional parton in $t\bar{t}j$ events, and not from the top decay products. Hence the top background is modeled with a tree level MC program for the process $pp \rightarrow t\bar{t}j \rightarrow W^+bW^-\bar{b}j$.

The three vector boson graph in $qq \rightarrow qqW$ is enhanced in the phase space region where the two final state quark jets emerge at very small angles. Hence events are tagged with one very forward and one very backward jet while the lepton originating from the $W \rightarrow \ell\nu$ decay is to be expected in the central region. Events are triggered by a charged lepton with $p_T(\ell) > 20$ GeV, and we require $p_T > 50$ GeV as a signature for W leptonic decays. On either side of the charged lepton (with respect to pseudorapidity) one then searches for the first hadronic jet with $p_T(j) > 40$ GeV and $|\eta(j)| < 5$, which will be called tagging jets and represent the two spectator quarks in our signal calculation. Leptons and jets are required to be well separated, $\Delta R(j, j) > 0.7$, $\Delta R(\ell, j) > 0.7$. The forward-backward nature of the two tagging jets is then taken into account by requiring $-5 < \eta(j_1) < -2.5$ and $2.5 < \eta(j_2) < 5$. Notice that this implies the existence of a central “rapidity gap”, at least 5 units wide in pseudorapidity, which contains the charged lepton but no jets with $p_T > 40$ GeV.

The above requirements leave a QCD Wjj background which is about a factor six larger than the remaining signal. However, the background is dominated by W -bremsstrahlung off initial or final state quarks. W -bremsstrahlung and the three vector boson graph lead to drastically different lepton pseudorapidity distributions for the signal and the background. The QCD Wjj background can thus be further suppressed by requiring $|\eta(\ell)| < 1.5$ and $\Delta\eta(\ell, j) = \min(|\eta(\ell) - \eta(j_1)|, |\eta(\ell) - \eta(j_2)|) > 2.5$. An additional strong background rejection is achieved by exploiting the very large dijet invariant masses, $m(jj)$, which are typical for the vector boson fusion process. A cut of $m(jj) > 3$ TeV, imposed on the two tagging jets, reduces the background well below signal level ($\sigma_{\text{SIG}} = 450$ fb vs. $\sigma_{\text{QCD}} = 136$ fb for the QCD Wjj background and $\sigma_{t\bar{t}j} = 38$ fb for $m_t = 140$ GeV).

The cuts discussed above single out the phase space region in which the electroweak fusion process dominates and hence one expects a pronounced sensitivity to deviations in the $WW\gamma$ and WWZ couplings from the SM prediction. Anomalous coupling effects are enhanced at large momentum transfer and, hence, for large transverse momenta of the produced W -boson. The effect is demonstrated in Fig. 6. While the p_{TW} distributions show similar shapes for the SM signal and the QCD and top quark backgrounds, a strong enhancement at large transverse momenta arises from anomalous couplings. For these three curves all other anomalous couplings are set to zero. Here the standard parameterization of the anomalous couplings in terms of C and P conserving anomalous couplings g_1^V , κ^V and λ^V , $V = \gamma, Z$ is used.

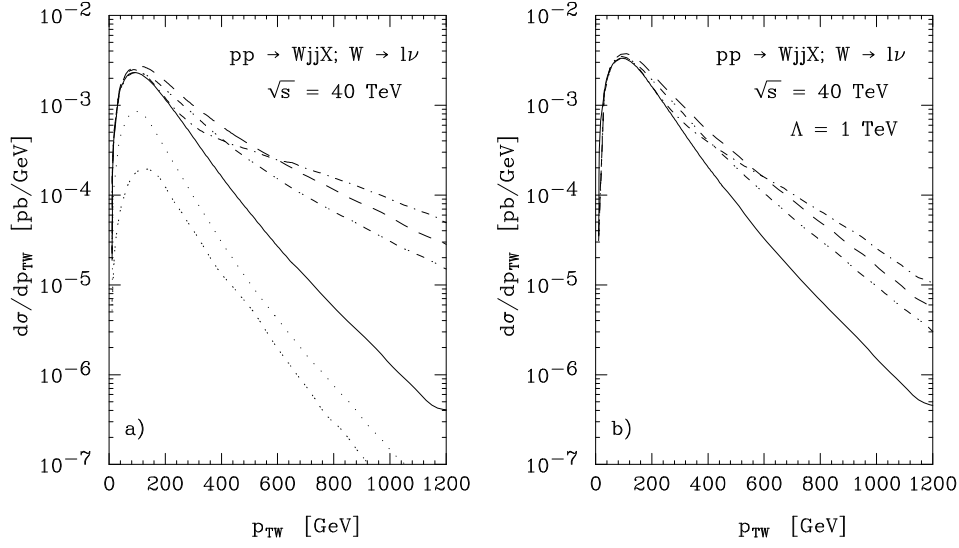


Figure 6: Transverse momentum distribution of the produced W -boson in Wjj events at the SSC. a) Individual distributions for the SM signal (solid line), the QCD Wjj background (dotted line) and the $t\bar{t}j$ background for $m_t = 140$ GeV (double dotted line). The upper three curves correspond to three choices of anomalous couplings: $\kappa^\gamma = \kappa^Z = 1.2$ (dashed line) $\lambda^\gamma = \lambda^Z = 0.1$ (dash-dotted curve) and $g_1^Z = 1.2$ (dash-double dotted line). b) The two background distributions have been added to the four signal curves. In addition the effect of a form-factor is shown for a scale $\Lambda = 1$ TeV. The cuts imposed are described in the text.

These couplings can be defined by the effective Lagrangian

$$i\mathcal{L}_{eff}^{WWV} = g_{WWV} \left(g_1^V (W_{\mu\nu}^\dagger W^\mu - W^{\dagger\mu} W_{\mu\nu}) V^\nu + \kappa^V W_\mu^\dagger W_\nu V^{\mu\nu} + \frac{\lambda^V}{m_W^2} W_{\rho\mu}^\dagger W^\mu{}_\nu V^{\nu\rho} \right), \quad (8)$$

where the overall coupling constants are defined as $g_{WW\gamma} = e$ and $g_{WWZ} = e \cot \theta_W$. Within the SM, at tree level, $g_1^Z = g_1^\gamma = \kappa^Z = \kappa^\gamma = 1$, and $\lambda^Z = \lambda^\gamma = 0$. g_1^γ is just the electric charge of the W and hence fixed to 1 by electromagnetic gauge invariance.

From Fig. 6b it can be seen that form factor effects are important in $qq \rightarrow qqW$. The results of a more quantitative analysis of the sensitivity of Wjj production to anomalous WWV couplings are described in Ref. [14]. The 2σ limits on $\kappa^V - 1$, λ^V and $\Delta g_1^Z = g_1^Z - 1$ are found to be in the $0.03 \dots 0.1$ range. Comparing these results with the limits obtained from di-boson production, one finds that the process $qq \rightarrow qqW$ is significantly more sensitive to $\Delta\kappa^V$ and Δg_1^Z than $W\gamma$ and WZ production for cutoff scales Λ in the low TeV range. In general, the pair production process is affected more by details of the form-factors. This emphasizes the need to measure Wjj production in addition to di-boson production if full information on the WWV couplings is to be gained.

5. Summary

The large statistics accumulated in the 1992-94 Tevatron runs will result in significantly improved measurements of the SM parameters. The energy distribution of the W decay electron offers an attractive alternative way to measure m_W . The large number of $W + 1$ jet events will make it possible to measure W plus charm production, which could help constraining the s -quark distribution function. Vector boson self-interactions are expected to be probed with 10 – 60% accuracy with the new Tevatron data. The lepton photon rapidity difference distribution will give easy access to the radiation zero predicted by the SM for $W\gamma$ production. $t\bar{t}\gamma$ production was found to be an important background to $W\gamma$ production at the SSC. However, it can be easily eliminated by a jet veto. Single W production via electroweak interactions at the SSC provides a measurement of the WWV vertices which is complementary to that in di-boson production.

6. References

1. L. Arnaudon *et al.*, CERN-PPE/93-53 (March 1993).
2. K. Hikasa *et al.* (Particle Data Group), *Phys. Rev.* **D45**, S1 (1992).
3. A. Peryshkin, these proceedings.
4. W. K. Tung, these proceedings.
5. A. D. Martin, R. G. Roberts and W. J. Stirling, *Phys. Rev.* **D47**, 867 (1993) and *Phys. Lett.* **B306**, 145 (1993), **B309**, 492(E) (1993).
6. J. Botts *et al.* (CTEQ Collaboration), *Phys. Lett.* **B304**, 159 (1993).
7. U. Baur *et al.*, these proceedings and FSU-HEP-930816 (preprint).
8. G. Landsberg, these proceedings.
9. U. Baur and D. Zeppenfeld, *Nucl. Phys.* **B308**, 127 (1988); U. Baur and E. L. Berger, *Phys. Rev.* **D41**, 1476 (1990), *Phys. Rev.* **D47**, 4889 (1993).
10. U. Baur, T. Han and J. Ohnemus, FSU-HEP-930519 preprint (May 1993), to appear in *Phys. Rev.* **D**.
11. see e.g. R. W. Brown, K. L. Kowalski, and S. J. Brodsky, *Phys. Rev.* **D28**, 624 (1983) and references therein.
12. U. Baur, S. Errede, and G. Landsberg, FSU-HEP-930727 (preprint, July 1993) and these proceedings.
13. U. Baur and A. Stange, FSU-HEP-930830 (preprint, August 1993) and these proceedings.
14. U. Baur and D. Zeppenfeld, FSU-HEP-930903 (preprint, September 1993) and these proceedings.
15. F. Abe *et al.* (CDF Collaboration), *Phys. Rev. Lett.* **70**, 4042 (1993).
16. H.-U. Bengtsson and T. Sjöstrand, *Comp. Phys. Commun.* **46**, 43 (1987).
17. J. Smith, D. Thomas, and W. L. van Neerven, *Z. Phys.* **C44**, 267 (1989); J. Ohnemus, *Phys. Rev.* **D47**, 940 (1993).

- 18. J. Gunion, *et al.*, *Phys. Lett.* **B163**, 389 (1985); J. Gunion and M. Soldate, *Phys. Rev.* **D34**, 826 (1986); W. J. Stirling *et al.*, *Phys. Lett.* **B163**, 261 (1985).
- 19. C. L. Bilchak *et al.*, *Phys. Rev.* **D29**, 375 (1984).
- 20. J. Alitti *et al.* (UA2 Collaboration), *Phys. Lett.* **B277**, 194 (1992).
- 21. U. Baur, S. Errede, and J. Ohnemus, FSU-HEP-930322 preprint (March 1993), to appear in *Phys. Rev.* **D**.
- 22. D. W. Duke and J. F. Owens *Phys. Rev.* **D26**, 1600 (1982).
- 23. E. L. Berger *et al.*, SDC Technical Design Report, SDC-92-201 (April 1992).